NJC

ROYAL SOCIETY OF CHEMISTRY

PAPER

Check for updates

Cite this: *New J. Chem.*, 2020, **44**, 11349

Improved synthesis of *N*-ethyl-3,7-bis(trifluoromethyl)phenothiazine†

Selin Ergun, Matthew D. Casselman, Aman Preet Kaur, N. Harsha Attanayake, Sean R. Parkin and Susan A. Odom *

Received 13th January 2020,
Accepted 28th May 2020

DOI: 10.1039/d0nj00184h

rsc.li/njc

N-Ethyl-3,7-bis(trifluoromethyl)phenothiazine is a highly soluble redox shuttle for overcharge protection in lithium-ion batteries with an oxidation potential of *ca.* 3.8 V *vs.* $Li^{+/0}$ in carbonate solvents. This compound has enabled extensive overcharge protection of $LiFePO_4$/graphite cells and does so at high charging rates at high concentrations. Our initial synthesis of this compound suffered from low yields and difficult purifications. Here we report a cleaner, higher-yielding synthesis and additional characterization of the product and its stable radical cation salt.

Introduction

The development of stable, electron-donating electro-active materials is important for numerous technological applications that involve reversible electron transfer reactions.[1–4] Of particular interest to electrochemical energy storage devices is their use as redox shuttles for overcharge protection of lithium-ion batteries (LIBs)[5–13] and as catholytes in non-aqueous redox flow batteries (RFBs).[14–31] Of the hundreds of compounds that have been tested for overcharge protection in LIBs, *N*-ethyl-3,7-bis(trifluoromethyl)phenothiazine (BCF_3EPT) is one of the most robust redox shuttles reported to date for full cells containing $LiFePO_4$ cathodes. This shuttle survives almost 250 cycles of 100% overcharge (200% charge) and for *ca.* 3400 h in constant charge when incorporated into $LiFePO_4$/graphite coin cells at 0.08 M in the electrolyte 1.2 M $LiPF_6$ in ethylene carbonate/ethyl methylcarbonate (3 : 7 wt. ratio) when charged at a rate of *C*/10.[32,33] At concentrations of 1.0–1.5 M, overcharge protection can be mitigated at higher charging currents (up to 1C) for a few hundred hours.[34] While cells operating in overcharge gradually lose capacity, they last longer in overcharging conditions when BCF_3EPT is added, and standard charge/discharge cycling is not hindered by the presence of this shuttle.

Because of its high solubility and stable radical cation, we performed preliminary screening tests for RFB applications.[23] The analysis showed that BCF_3EPT is not only stable in carbonate-based electrolytes but also in other non-aqueous electrolytes that have been utilized in RFBs containing organic active materials, for example, acetonitrile (ACN). The redox potential of 3.83 V *vs.* $Li^{+/0}$ makes BCF_3EPT among the highest potential organic compounds that possess both high solubility and stability in multiple redox states. An examination of the reversibility of the first oxidation in ACN-based electrolytes shows that the redox event exhibits high reversibility and fast electron-transfer kinetics (see an example in Fig. S1, ESI†). Furthermore, using UV-vis absorption spectroscopy to monitor stability of the radical cation form of BCF_3EPT in solution. The radical cation showed negligible decay at 10 mM in ACN and in ACN-based electrolytes over several hours at room temperature (see an example in Fig. S2, ESI†).

Due to the combination of extensive performance in overcharge protection and in RFB screening studies, a scaled up synthesis of BCF_3EPT would enable a wider array of experiments to be performed. Our original preparation of BCF_3EPT was accomplished in three steps from phenothiazine: (1) alkylation with bromoethane, (2) aromatic bromination with *N*-bromosuccinimide, and (3) bis(trifluoromethylation) with potassium trifluoroacetate and copper(I) iodide catalyst (Scheme 1).[32,33] While the first two reactions were high-yielding, the bis(trifluoromethylation) suffered from a low yield of 22%.[33] Thus, we sought to optimize the synthesis of BCF_3EPT, using additives and co-solvents to increase reaction yield and purity. In addition to these variations in reaction conditions, the single crystal X-ray structures of the neutral compound and its $SbCl_6$-based radical cation salt are reported, the isolation of which demonstrates the high stability of this singly oxidized state. Further, thermal stability is reported due to the potential use of BCF_3EPT and related trifluoromethylated phenothiazines as solid-state semiconductors.

Department of Chemistry, University of Kentucky, Lexington, KY 40502, USA. E-mail: susan.odom@uky.edu

† Electronic supplementary information (ESI) available: Cyclic voltammetry experiments, synthesis of BCF_3EPT precursors, synthesis and UV-vis stability studies of the BCF_3EPT-BF_4, NMR spectra, thermal ellipsoid plots from X-ray crystallography. CCDC 1482195 and 1482196. For ESI and crystallographic data in CIF or other electronic format see DOI: 10.1039/d0nj00184h

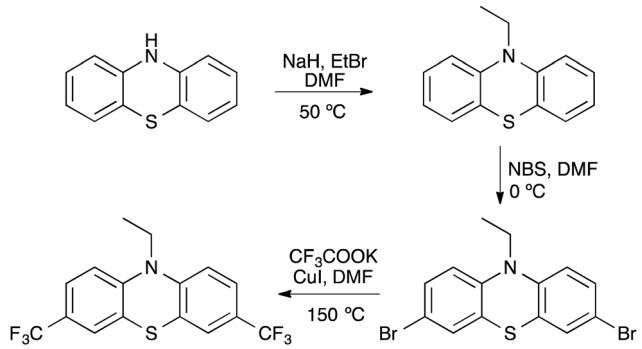

Scheme 1 Reagents used in our original, three-step synthesis of *N*-ethyl-3,7-bis(trifluoromethyl)phenothiazine (BCF_3EPT).

Results and discussion

The use of potassium trifluoroacetate/copper(I) iodide mediated trifluoromethylation of 3,7-dibromo-*N*-ethylphenothiazine (DBrEPT) in NMP affords BCF_3EPT in modest yield and purity.[33–35] In addition to the low conversion to desired product, the formation of side-products makes the purification of BCF_3EPT challenging. Incomplete substitution products such as $BrCF_3EPT$ and CF_3EPT (Fig. 1) are often observed, although these products are easily separated from desired products by column chromatography. However, the byproduct $(CF_3)(C_2F_5)EPT$ (Fig. 1) – produced by decomposition of trifluormethylation reagents – is difficult to remove by column chromatography due to the similar retention factors of BCF_3EPT and $(CF_3)(C_2F_5)EPT$ on silica and alumina gels. While $(CF_3)(C_2F_5)EPT$ and BCF_3EPT may be similarly effective as redox shuttles or battery active materials, the unknown behaviour of $(CF_3)(C_2F_5)EPT$ provides motivation to separate it from the desired product.

It may be possible to prepare BCF_3EPT from commercially available precursors containing CF_3 groups. However, we decided against this route because (1) the number of synthetic operations would increase from our original three steps to five, and (2) due to already having optimized the first two synthetic steps with yields above 90% in a few-dozen gram scales using low-cost reagents; only the third step needed optimization. Thus the original scheme was retained with a plan to optimize the final step – the bis(trifluoromethylation) of DBrEPT and evaluated different trifluoromethylating reagents to determine if the reaction yield could be increased and the formation of the pentafluoroethyl-containing side product $(CF_3)(C_2F_5)EPT$ suppressed.

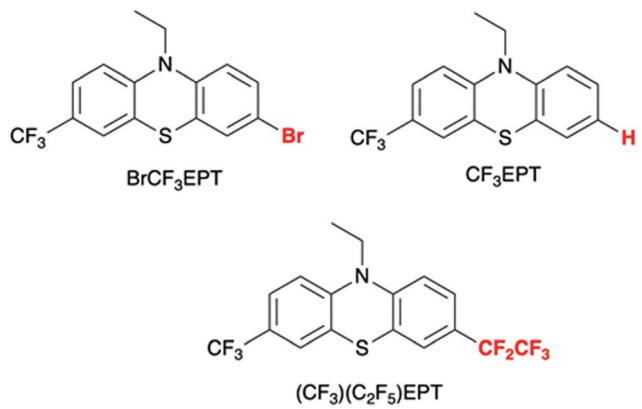

Fig. 1 Incomplete transformations and byproducts formed during the conversion of 3,7-dibromo-*N*-ethylphenothiazine (DBrEPT) to *N*-ethyl-3,7-bis(trifluoromethyl)phenothiazine (BCF_3EPT) using potassium trifluoroacetate and copper(I) iodide.

A variety of reagents have been used to convert aryl halides to their CF_3-substituted equivalents. Inspired by the work of Grushin,[36] Buchwald,[37] Amii,[38] and others who utilized copper and palladium catalysts in tandem with the trifluoromethylating reagents, we attempted the conversion of DBrEPT to BCF_3EPT with trimethyltrifluoromethylsilane ($(CH_3)_3SiCF_3$) or triethyltrifluoromethylsilane ($(CH_3CH_2)_3SiCF_3$) along with a metal fluoride salt (CsF or KF) as the sources of CF_3^- with the catalyst/ligand combinations $[PdCl(allyl)]_2$/Brettphos and copper(I) iodide/phenanthroline. While these catalyst systems have been successful in the monotrifluoromethylation of a variety of substrates, these reactions are most efficient with electron-poor substrates. With electron-rich DBrEPT, low yields of the desired product resulted due to low percent conversion of the starting DBrEPT, even for prolonged reaction times. Similarly, attempts to accomplish trifluoromethylation with a combination of methyl trifluoroacetate, cesium fluoride, and copper(I) iodide resulted in no undesired $(CF_3)(C_2F_5)EPT$, but the yield of desired BCF_3EPT was low (5–30%), and significant amounts of CF_3EPT (17–53%) were observed. Disappointed with the performance of alternative CF_3 sources, it seemed reasonable to optimize the trifluoromethylation with the original reagent system: potassium trifluoroacetate and copper iodide.

Because separation of BCF_3EPT and $(CF_3)(C_2F_5)EPT$ is not trivial, it is necessary to optimize reaction conditions to minimize the amount of $(CF_3)(C_2F_5)EPT$ formed. Pentafluoroethyl-substituted products result from the formation of pentafluoroethyl copper species in the reaction mixture. This is a known by-product of trifluoromethylation reactions and is thought to be due to the instability of the trifluoromethyl anion.[39–42] A number of strategies have been used to stabilize this reactive species including the use of DMF[39–43] and metals[40,44,45] as additives. The trifluoromethyl anion is thought to fragment to form fluoride and difluorocarbene, the latter of which reacts with another trifluoromethyl anion to form the pentafluoroethyl copper,[43,46] leading to undesired byproducts (Scheme 2).

Following our original conditions employed to convert DBrEPT to BCF_3EPT, analysis of product components post-workup using gas chromatography/mass spectrometry (GCMS) to identify in what cases the ratio of BCF_3EPT to $(CF_3)(C_2F_5)EPT$ increased and where the overall amount of BCF_3EPT increased. The GCMS traces are shown in Fig. 2 and results are summarized in Table 1. In our first attempt, DBrEPT (0.06 M) was combined with 5 equivalents of potassium trifluoroacetate and 5 equivalents of copper(I) iodide in *N*-methylpyrrolidinone (NMP) in an air-free flask, which was heated for 48 h (entry 1, Table 1) at 180 °C. The addition of 1,3-dimethyl-2-imidazolidinone (DMI) as a co-solvent resulted in increasing amounts of the desired product and diminished

 This journal is © The Royal Society of Chemistry and the Centre National de la Recherche Scientifique 2020

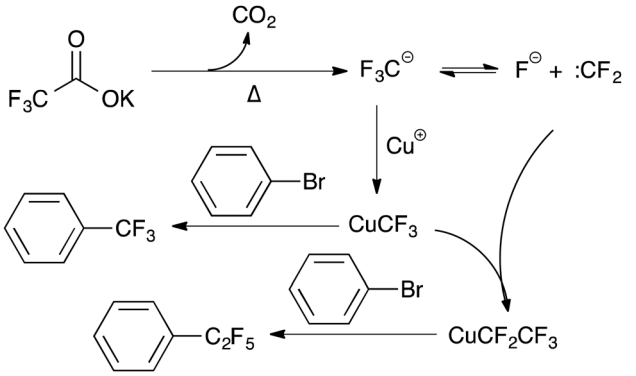

Scheme 2 Postulated mechanism for trifluoromethylation and formation of pentafluoroethyl side products.

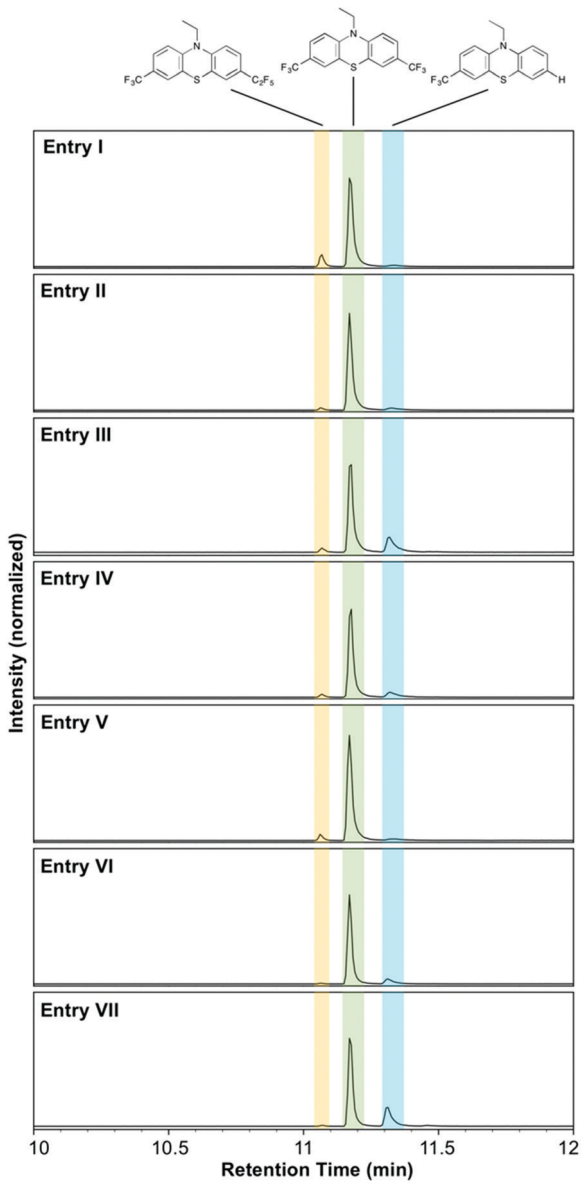

Fig. 2 GCMS traces and corresponding structures for the observed peaks.

amounts of $(CF_3)(C_2F_5)$EPT (entry II, Table 1). The addition of CsF as an additive also had a beneficial effect on product distribution; however, lower conversion was noted (entry III, Table 1). Using CsF and DMI together had a synergistic effect with both high yield of desired product and low by-product formation (entry IV, Table 1). Increasing CuI concentration increased the yield of both desired and undesired products (entry V), while decreasing the CF_3COOK concentration decreased the amount of $(CF_3)(C_2F_5)$EPT formed to less than 1% as determined by GC/MS (entries VI and VII, Table 1). We hypothesize that CsF drives the difluorocarbene/trifluoromethyl anion equilibrium towards the trifluoromethyl anion, thus reducing the amount of pentafluoroethyl copper formed.

From the optimized conditions shown in Table 1 for entry VI, an increase in the scale of reaction to 5 mmol (10 times the scale used for optimization) is reported. On this 5 mmol scale, the isolated yield was 70%, more than 3 times higher than our original synthesis. Over the three steps required to obtain the product, the overall yield is 58%.

^1H, ^{13}C, and ^{19}F NMR spectra of isolated BCF_3EPT demonstrate the lack of observable impurities in the product (Fig. S1, ESI†). The ^1H NMR spectrum shows two doublets and a singlet in the aromatic region as well as a signal for residual $CHCl_3$ in $CDCl_3$. The ethyl group is found in the aliphatic region with a quartet for the methylene (CH_2) group at 3.97 ppm and a triplet for methyl (CH_3) group at 1.44 ppm. The ^{13}C NMR spectrum is complicated by short- and long-range carbon–fluorine coupling. The trifluoromethyl carbons (centered at 123.9 ppm) are split into a large quartet ($^1J_{CF}$ = 271 Hz) that overlaps with the aromatic carbons. Two and three bond C–F couplings also complicate the ^{13}C NMR spectra; the carbon *ipso* to CF_3 has $^2J_{CF}$ = 33.3 Hz and the carbons *ortho* to CF_3 have $^3J_{CF}$ = 3.8 Hz. The ^{19}F NMR spectrum shows one singlet at −62.2 ppm – the most important feature that shows that the product is pure BCF_3EPT without residual CF_3EPT, $BrCF_3$EPT, or $CF_3C_2F_5$EPT – which would give rise to additional signals in this spectrum. The ^{19}F NMR is key in determining purity of BCF_3EPT, as pentafluoroethyl side-products are not easily identifiable by either ^1H or ^{13}C NMR.

Single crystal X-ray structures provide definitive proof of product identity. The view of the π face (Fig. S4a, ESI†) shows the connectivity of C, N, S, and F atoms. The phenothiazine ring system is bent through the S and N atoms, giving either a 145.5° or 152.1° angle as defined by planes through the C atoms in each of the two aromatic rings. As our group recently reported,[47] the structure of BCF_3EPT predicted by density functional theory (DFT) calculations at the B3LYP/6-311G(d,p) level of theory has a butterfly angle of 139.7°. The $SbCl_6$-based radical cation salt of BCF_3EPT was also prepared and crystallized to determine the geometry when oxidized. The butterfly angle as determined by X-ray crystal structure was 164.5° (Fig. S4b, ESI†), which is in good agreement with the DFT-calculated value of 171.1°.[47]

The crystal packing of triclinic neutral BCF_3EPT shows that layers of two-dimensional ribbons stack atop one another (Fig. 3a). No significant π–π interactions are present in this crystal; the closest interactions are fluorine–fluorine and fluorine–hydrogen (hydrogen from methylene group) distances of 2.91 and 2.64 Å, respectively. The concentration of the solid can be calculated

Table 1 Amounts of reagents used and percent abundance of the products for selected experiments. For each trial the concentration of DBrEPT was 0.06 M, and was run on a 0.5 mmol scale. All trials were run in air-free flasks

					% abundance by GCMS			
Trial	CF_3CO_2K (eq.)	CuI (eq.)	CsF (eq.)	DMI/NMP ratio	BCF_3EPT	$CF_3C_2F_5EPT$	CF_3EPT	$BrCF_3EPT$
I	5	5	—	0 : 9	87.2	10.0	2.9	0
II	5	5	—	2 : 7	92.4	2.1	5.6	0
III	5	5	2	0 : 9	75.7	3.4	20.9	0
IV	5	5	2	2 : 7	87.2	2.7	10.1	0
V	5	7	2	2 : 7	91.1	4.6	4.3	0
VI	4	7	2	2 : 7	89.6	0.8	9.6	0
VII	4	5	2	2 : 7	73.2	0.7	23.9	2.1

using the molecular weight of the compound and its density. At 363.32 g mol^{-1} and a density of 1.624 g cm^{-3}, the concentration/volume density is 4.47 M. In the radical cation crystal, which packs in a monoclinic space group, phenothiazine units are farther apart from one another, with the closest fluorine–fluorine bond having a distance of 3.43 Å (Fig. 3b). The closest fluorine–hydrogen distance is 2.93 Å, where the hydrogen atom is part of the methyl group; the closest gap between a fluorine atom and a methylene hydrogen is 4.96 Å.

Weak interactions in the solid state give the BCF_3EPT crystal a low melting point. The differential scanning calorimetry scan is shown in Fig. 4a. A crystalline sample of BCF_3EPT was heated to 200 °C at 10° min^{-1}, then cooled to −40 °C at the same rate, then heated again to 200 °C. In both heating cycles, a melting transition occurred at 69 °C. It appears that in the second heating cycle, a glass transition occurred at −27 °C. Then, before melting, a few exothermic peaks appear, which may correspond to a crystallization of the semi-solid, enabled by increased thermal energy. Thermogravimetric analysis (Fig. 4b) under nitrogen atmosphere shows the mass of BCF_3EPT at increasing temperatures. At *ca.* 170 °C, the sample began to lose mass, and by 240 °C, no measurable sample mass remained. From this experiment, it was not possible to know if the mass loss was due to evaporation or decomposition. To determine the reason for mass loss, *ca.* 280 mg of the sample was heated to 300 °C in a test tube under nitrogen atmosphere. While heating the bottom of the test tube, the sample migrated from bottom of the tube to its walls. Irradiation of the sample with UV light showed the blue fluorescence characteristic of the compound in the material that condensed on the walls of the tube, suggesting that the sample evaporated without significant decomposition.

Experimental

Materials and methods

Sodium hydride, phenothiazine, *N*-bromosuccinimide (NBS), and copper(I) iodide were purchased from Acros Organics. Bromoethane was purchased from Sigma Aldrich. Potassium trifluoroacetate and cesium fluoride were purchased from Oakwood Chemical. Anhydrous solvents *N*,*N*-dimethylformamide (DMF), *N*-methylpyrrolidone (NMP), and 1,3-dimethyl-2-imidazolidinone (DMI) were purchased from Acros Organics. *N*-Bromosuccinimide was freshly crystallized from water prior to use. Potassium trifluoroacetate was vacuum dried prior to each use. All the other reagents were used without further purification. Silica gel (230 × 400 mesh) was purchased from Silicycle, and solvents for purification were purchased from Fisher Scientific. ^1H, ^{13}C, and ^{19}F NMR spectra were obtained on Varian spectrometers in DMSO-d_6 or $CDCl_3$ from Cambridge Isotope Laboratories. Mass spectra were obtained on an Agilent 5973 Network mass selective detector attached to Agilent 6890N Network GC system.

Synthetic procedures

The synthesis of EPT and DBrEPT on 50 and 20 gram scales, respectively, is described in the ESI.†

Experimental details for results presented in Table 1. DBrEPT (0.193 g, 0.501 mmol), CF_3COOK (0.304 g, 2.00 mmol or 0.380 g, 2.50 mmol) and CuI (0.476 g, 2.50 mmol or 0.667 g, 3.50 mmol) were added to an oven-dried 20 mL air-free flask under nitrogen atmosphere. CsF (none or 0.152 g, 1.00 mmol) was added under inert atmosphere in a glovebox. Anhydrous NMP (7 mL or 9 mL) and DMI (0 mL or 2 mL) were added to the reaction mixture, and the flask was immersed in an oil bath preheated to 90 °C flask after which the reaction mixture was sparged with N_2 for 10 min. The pressure flask was sealed, the temperature increased to 180 °C, and the reaction was stirred for 48 h. Upon completion, the reaction flask was removed from the oil bath and allowed to cool to rt, then and poured onto Celite in hexanes and then vacuum filtered while washing with hexanes. The filtrate was washed with water and the organic layer was dried over $MgSO_4$ and filtered. GCMS data were collected from crude extracts. The organic extracts were concentrated by rotary evaporation to afford the product as a yellow oil.

Experimental details for 5 mmol scale using optimized conditions. DBrEPT (1.93 g, 5.00 mmol, 1 eq.), CF_3COOK (3.04 g, 20.0 mmol, 4 eq.) and CuI (6.67 g, 35.0 mmol, 7 eq.) were added to an oven-dried 150 mL pressure vessel under nitrogen atmosphere. The vessel was brought into an argon-filled glovebox where CsF (1.52 g, 10.0 mmol, 2 eq.) was added. Anhydrous NMP (70 mL) and DMI (20 mL) were added to the reaction mixture, and the pressure flask was purged with nitrogen for 10 min in an oil bath preheated to 90 °C. The pressure flask was sealed, the temperature was increased to 180 °C, and the reaction was stirred for 48 h. Upon completion, the reaction was cooled and poured onto Celite in hexanes, and then vacuum filtered while washing with hexanes. The filtrate was washed twice with water, and the organic layer was dried over $MgSO_4$ and filtered to remove solids. The organic extracts

 This journal is © The Royal Society of Chemistry and the Centre National de la Recherche Scientifique 2020

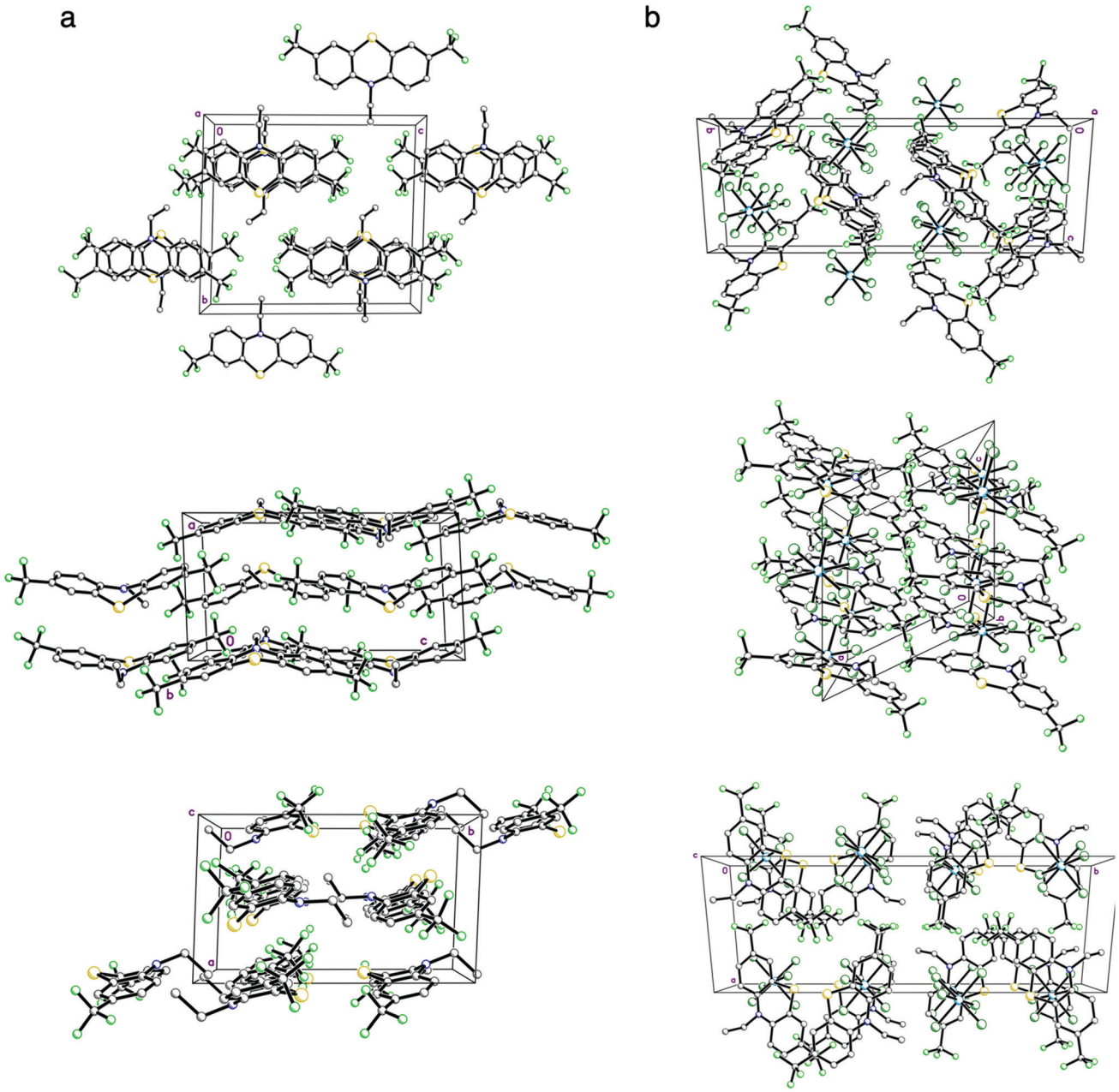

Fig. 3 Solid-state packing of neutral BCF_3EPT (a) and BCF_3EPT-$SbCl_6$ (b) from their X-ray crystal structures. In image (b), the $SbCl_6^-$ anions are omitted for clarity.

were concentrated by rotary evaporation to afford the product as a yellow oil. The crude product was purified by column chromatography with cyclohexane/Et_2O (16 : 1) as the eluent to afford 1.26 g (70%) of the product. BCF_3EPT was isolated as a yellow oil, which solidified over *ca.* 8 h at rt. Crystals suitable for X-ray analysis were prepared by slow evaporation from ethanol. ^1H NMR (400 MHz, $CDCl_3$) δ (ppm) 7.41–7.39 (m, 2H), 7.33 (m, 2H), 6.91 (d, J = 8.6 Hz, 2H), 3.97 (q, J = 7 Hz, 2H), 1.44 (m, 3H). ^{13}C NMR (100 MHz, $CDCl_3$) δ (ppm): 146.9, 123.9 (q, J_{CF} = 271.2 Hz), 125.3 (q, J_{CF} = 33.0 Hz), 124.9 (q, J_{CF} = 3.8 Hz), 124.3 (q, J_{CF} = 3.8 Hz), 124.2, 42.4, 12.7. GCMS: m/z 363 (44%), 348 (14%), 334 (100%), 316 (12%).

Synthesis of *N*-ethyl-3,7-bis(trifluoromethyl)phenothiazinium hexachloroantimonate (BCF_3EPT-$SbCl_6$). BCF_3EPT (370 mg, 1.02 mmol, 1 eq.) was dissolved in DCM (8 mL) under nitrogen in a round-bottom flask fitted with a rubber septum after which the reaction mixture was cooled to 0 °C by immersing the reaction flask into an ice water bath. $SbCl_5$ (200 μL, 1.57 mmol, 1.5 eq.) was added dropwise with stirring, which resulted in a brown solution. After 10 min, hexanes (60 mL) was added, and a brown solid precipitate formed. The resulting solid was filtered through a fritted glass funnel and washed with cold hexanes to afford 709 mg of the radical cation salt (99% crude yield). Crystals suitable for X-ray analysis were prepared by vapor diffusion from DCM and pentane at −20 °C.

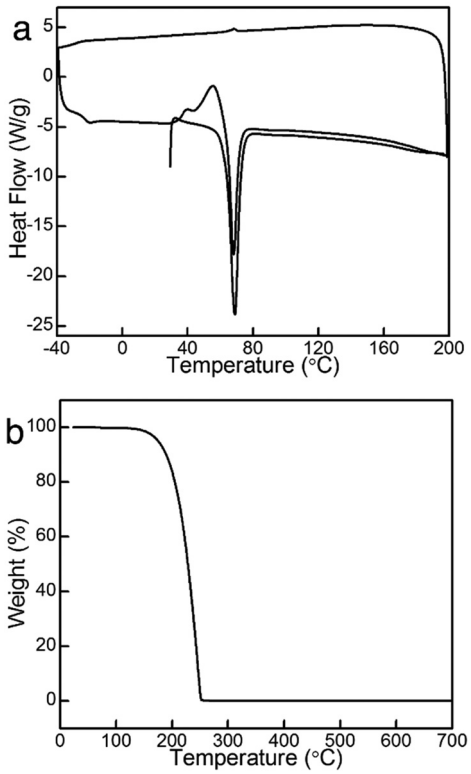

Fig. 4 Differential scanning calorimetry (DSC) traces (a) and thermal gravimetric analysis (TGA) traces (b) for BCF_3EPT under nitrogen.

Crystallography

X-ray diffraction data were collected on either a Nonius kappaCCD diffractometer (MoKα X-rays) or a Bruker-Nonius X8 Proteum (CuKα X-rays). Raw data were integrated using the Denzo-SMN package[48] (kappaCCD) or by APEX2 (X8 Proteum).[49] Scaling and merging for all datasets were performed using SADABS.[50] All structures were solved using SHELXT[51] and refined with SHELXL-2014/7.[52] Hydrogen atoms were included using the riding-model approximation. Non-hydrogen atoms were refined with anisotropic displacement parameters. Atomic scattering factors were taken from the International Tables for Crystallography, vol. C.[53]

For neutral BCF_3EPT, this crystal was one of two polymorphs present. The other component was orthorhombic (either *Pnma* or $Pna2_1$), with similar cell axis lengths to this triclinic variant. The orthorhombic crystals underwent a destructive phase transition on cooling below room temperature. That structure was solved, and was chemically identical to the triclinic form, but there was a lot of diffuse scatter in the diffraction pattern, and refinement was unsatisfactory. The triclinic crystals described here had none of the problems associated with the orthorhombic polymorph.

Differential scanning calorimetry and thermogravimetric analysis

The TGA experiment was performed on a TA Q5000 instrument, with a standard heating rate of 10 °C min^{-1} from room temperature to 700 °C under nitrogen atmosphere with a sample of size 8 mg. The DSC experiment was carried out on a DSC Q20 coupled with refrigerated cooling system under N_2 atmosphere using a heat/cool/heat procedure. The sample was heated at 10 °C min^{-1} from room temperature to 200 °C and then cooled to −40 °C at 10 °C min^{-1} and again heated to 200 °C at 10 °C min^{-1}.

Conclusions

In conclusion, after numerous trials and variations in chemical reagents, we report an improved synthesis of the robust, highly soluble redox shuttle BCF_3EPT and have prepared the compound in three steps, with an overall yield of 58% (*versus* 18% previously reported). Nuclear magnetic resonance spectroscopy, mass spectrometry, and X-ray crystallography confirm the identification and purity of the product. This low-melting solid is crystalline and is soluble at concentrations of 1.5 M in carbonate solvents containing lithium salts. Its extensive overcharge protection highlights its application as a redox shuttle for LIBs, and its stability in this application may allow it to serve as a robust electron donor in other electrochemical energy storage and semiconductor applications such as serving as the catholyte in RFBs or the hole-transport layer in field-effect transistors.

One aspect of future work will focus on tailoring the solubility of the radical cation form, with a particular emphasis on solvents and supporting electrolytes that are commonly utilized in electrochemical energy storage solutions, such as nitrile and carbonate solvents, and fluorinated and sulfonated anions. Further, while the trifluoromethylation of this phenothiazine core has been improved, the large-scale synthesis of BCF_3EPT is still an ardorous task.

Conflicts of interest

There are no conflicts to declare.

Acknowledgements

We thank the National Science Foundation, Division of Chemistry for Award Numbers CHE-1300653 and CHE-1800482, and from support through an NSF EPSCoR grant, Award Number 1355438. Further, we the NSF for support through a Major Research Instrumentation grant through Award Number CHE-1626732.

References

1 N. J. Treat, H. Sprafke, J. W. Kramer, P. G. Clark, B. E. Barton, J. Read de Alaniz, B. P. Fors and C. J. Hawker, *J. Am. Chem. Soc.*, 2014, **136**, 16096–16101.
2 E. H. Discekici, N. J. Treat, S. O. Poelma, K. M. Mattson, Z. M. Hudson, Y. Luo, C. J. Hawker and J. R. de Alaniz, *Chem. Commun.*, 2015, **51**, 11705–11708.
3 Z. Chen, Y. Qin and K. Amine, *Electrochim. Acta*, 2009, **54**, 5605–5613.
4 M. J. Lacey, J. T. Frith and J. R. Owen, *Electrochem. Commun.*, 2013, **26**, 74–76.

 This journal is © The Royal Society of Chemistry and the Centre National de la Recherche Scientifique 2020

5 J. Chen, C. Buhrmester and J. R. Dahn, *Electrochem. Solid-State Lett.*, 2005, **8**, A59–A62.
6 C. Buhrmester, L. Moshurchak, R. L. Wang and J. R. Dahn, *J. Electrochem. Soc.*, 2006, **153**, A288–A294.
7 C. Buhrmester, L. M. Moshurchak, R. L. Wang and J. R. Dahn, *J. Electrochem. Soc.*, 2006, **153**, A1800–A1804.
8 L. M. Moshurchak, C. Buhrmester and J. R. Dahn, *J. Electrochem. Soc.*, 2008, **155**, A129–A131.
9 W. Weng, J. Huang, I. A. Shkrob, L. Zhang and Z. Zhang, *Adv. Energy Mater.*, 2016, **6**, 1600795.
10 S.-L. Khakani, J. C. Forgie, D. D. MacNeil and D. Rochefort, *J. Electrochem. Soc.*, 2015, **162**, A1432–A1438.
11 S. A. Odom, A. Kaur, S. Ergun, C. F. Elliott and M. D. Casselman, *MRS Online Proc. Libr.*, 2015, **1740**, mrsf14-1740-z10-03, DOI: 10.1557/opl.2015.1204.
12 A. P. Kaur, C. F. Elliott, S. Ergun and S. A. Odom, *J. Electrochem. Soc.*, 2016, **163**, A1–A7.
13 A. P. Kaur, M. D. Casselman, C. F. Elliott, S. R. Parkin, C. Risko and S. A. Odom, *J. Mater. Chem. A*, 2016, **4**, 5410–5414.
14 J. Zhang, I. A. Shkrob, R. S. Assary, R. J. Clark, R. E. Wilson, S. Jiang, Q. J. Meisner, L. Zhu, B. Hu and Z. Zhang, *Materials Today Energy*, 2019, **13**, 308–311.
15 F. R. Brushett, J. T. Vaughey and A. N. Jansen, *Adv. Energy Mater.*, 2012, **2**, 1390–1396.
16 S.-H. Shin, S.-H. Yun and S.-H. Moon, *RSC Adv.*, 2013, **3**, 9095–9116.
17 W. Weng, Y. Tao, Z. Zhang, P. C. Redfern, L. A. Curtiss and K. Amine, *J. Electrochem. Soc.*, 2013, **160**, A1711–A1715.
18 D. Aaron, F. Delnick, C.-N. Sun, J. Nanda and T. A. Zawodzinski, *ECS Trans.*, 2014, 2398, Abstract MA2014–2001.
19 S. H. Oh, C. W. Lee, D. H. Chun, J. D. Jeon, J. Shim, K. H. Shin and J. H. Yang, *J. Mater. Chem. A*, 2014, **2**, 19994–19998.
20 J. Huang, L. Cheng, R. S. Assary, P. Wang, Z. Xue, A. K. Burrell, L. A. Curtiss and L. Zhang, *Adv. Energy Mater.*, 2015, **5**, 1401782.
21 J. Huang, L. Su, J. A. Kowalski, J. L. Barton, M. Ferrandon, A. K. Burrell, F. R. Brushett and L. Zhang, *J. Mater. Chem. A*, 2015, **3**, 14971–14976.
22 B. Hwang, M.-S. Park and K. Kim, *ChemSusChem*, 2015, **8**, 310–314.
23 A. P. Kaur, N. E. Holubowitch, S. Ergun, C. F. Elliott and S. A. Odom, *Energy Technol.*, 2015, **3**, 476–480.
24 X. Wei, L. Cosimbescu, W. Xu, J. Z. Hu, M. Vijayakumar, J. Feng, M. Y. Hu, X. Deng, J. Xiao, J. Liu, V. Sprenkle and W. Wang, *Adv. Energy Mater.*, 2015, **5**, 1400678.
25 X. Wei, W. Xu, J. Huang, L. Zhang, E. Walter, C. Lawrence, M. Vijayakumar, W. A. Henderson, T. Liu, L. Cosimbescu, B. Li, V. Sprenkle and W. Wang, *Angew. Chem., Int. Ed.*, 2015, **54**, 8684–8687.
26 L. Su, J. A. Kowalski, K. J. Carroll and F. R. Brushett, in *Rechargeable Batteries: Materials, Technologies and New Trends*, ed. Z. Zhang and S. S. Zhang, Springer International Publishing, Cham, 2015, pp. 673–712, DOI: 10.1007/978-3-319-15458-9_24.
27 E. V. Carino, J. Staszak-Jirkovsky, R. S. Assary, L. A. Curtiss, N. M. Markovic and F. R. Brushett, *Chem. Mater.*, 2016, **28**, 2529–2539.
28 W. Duan, R. S. Vemuri, J. D. Milshtein, S. Laramie, R. D. Dmello, J. Huang, L. Zhang, D. Hu, M. Vijayakumar, W. Wang, J. Liu, R. M. Darling, L. Thompson, K. Smith, J. S. Moore, F. R. Brushett and X. Wei, *J. Mater. Chem. A*, 2016, **4**, 5448–5456.
29 J. D. Milshtein, A. P. Kaur, M. D. Casselman, J. A. Kowalski, S. Modekrutti, P. Zhang, N. H. Attanayake, C. F. Elliott, S. R. Parkin, C. Risko, F. R. Brushett and S. A. Odom, *Energy Environ. Sci.*, 2016, **9**, 3531–3543.
30 Y. Yan, S. G. Robinson, M. S. Sigman and M. S. Sanford, *J. Am. Chem. Soc.*, 2019, **141**, 15301–15306.
31 N. H. Attanayake, J. Kowalski, K. V. Greco, M. D. Casselman, J. Milshtein, S. Chapman, S. R. Parkin, F. R. Brushett and S. A. Odom, *Chem. Mater.*, 2019, **31**, 4353–4363.
32 A. P. Kaur, S. Ergun, C. F. Elliott and S. A. Odom, *J. Mater. Chem. A*, 2014, **2**, 18190–18193.
33 S. Ergun, C. F. Elliott, A. P. Kaur, S. R. Parkin and S. A. Odom, *Chem. Commun.*, 2014, **50**, 5339–5341.
34 A. P. Kaur, C. F. Elliott, S. Ergun and S. A. Odom, *J. Electrochem. Soc.*, 2015, **163**, A1–A7.
35 S. A. Odom, S. Ergun, P. P. Poudel and S. R. Parkin, *Energy Environ. Sci.*, 2014, **7**, 760–767.
36 V. V. Grushin and W. J. Marshall, *J. Am. Chem. Soc.*, 2006, **128**, 12644–12645.
37 E. J. Cho and S. L. Buchwald, *Org. Lett.*, 2011, **13**, 6552–6555.
38 M. Oishi, H. Kondo and H. Amii, *Chem. Commun.*, 2009, 1909–1911.
39 B. R. Langlois and T. Billiard, *Synthesis*, 2003, 185–194.
40 S. Roy, B. T. Gregg, G. W. Gribble, V.-D. Le and S. Roy, *Tetrahedron*, 2011, **67**, 2161–2195.
41 G. Landelle, A. Panossian, S. Pazenok, J.-P. Vors and F. R. Leroux, *Beilstein J. Org. Chem.*, 2013, **9**, 2476–2536.
42 A. Lishchynskyi, M. A. Novikov, E. C. Escudero-Adan, P. Novak and V. V. Grushin, *J. Org. Chem.*, 2013, **78**, 11126–11146.
43 O. A. Tomashenko, E. C. Escudero-Adan, M. M. Belmonte and V. V. Grushin, *Angew. Chem., Int. Ed.*, 2011, **50**, 7655–7659.
44 Y. Nakamura, M. Fujiu, T. Murase, Y. Itoh, H. Serizawa, K. Aikawa and K. Mikami, *Beilstein J. Org. Chem.*, 2013, **9**, 2404–2409.
45 T. Knauber, F. Arikan, G.-V. Roschenthaler and L. J. Goossen, *Chem. – Eur. J.*, 2011, **17**, 2689–2697.
46 D. M. Wiemers and D. J. Burton, *J. Am. Chem. Soc.*, 1986, **108**, 832–834.
47 M. D. Casselman, C. F. Elliott, S. Modekrutti, P. Zhang, S. R. Parkin, C. Risko and S. A. Odom, *ChemPhysChem*, 2017, **18**, 2142–2146.
48 Z. Otwinowski and W. Minor (1997) *Methods in Enzymology 276 part A*, ed. C. W. Carter, Jr. and R. M. Sweet, Academic Press, pp. 307–326.
49 Bruker-AXS (2006). *APEX2*, Bruker-AXS Inc., Madison, WI, USA.
50 L. Krause, R. Herbst-Irmer, G. M. Sheldrick and D. Stalke, *J. Appl. Crystallogr.*, 2015, **48**, 3–10.
51 G. M. Sheldrick, *Acta Crystallogr.*, 2015, **A71**, 3–8.
52 G. M. Sheldrick, *Acta Crystallogr.*, 2015, **C71**, 3–8.
53 *International Tables for Crystallography*, ed. A. J. C. Wilson, Kluwer Academic Publishers, Holland, vol. C, 1992.